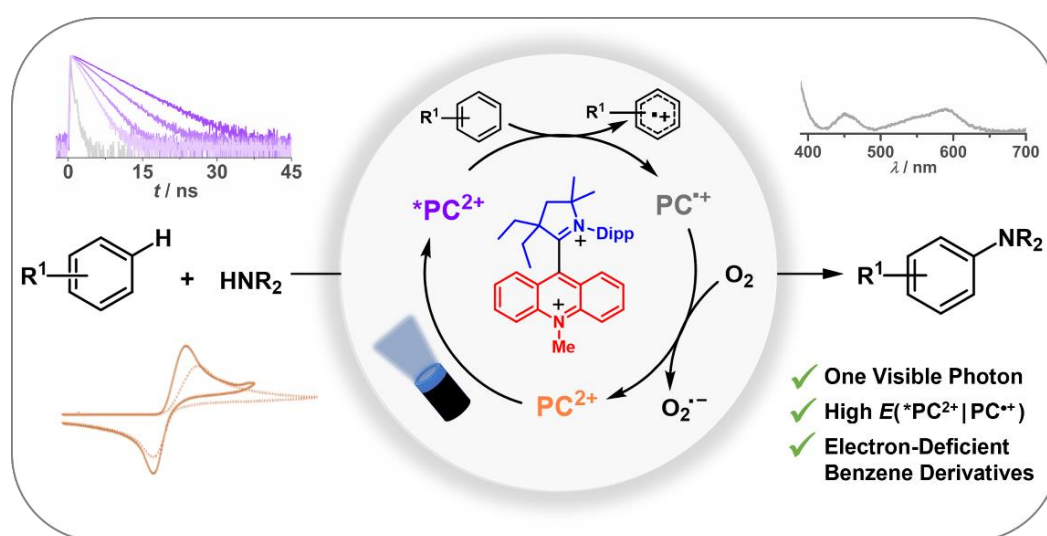# Dicationic Acridinium/Carbene Hybrids as Strongly Oxidizing Photocatalysts

Samaresh C. Sau,[a] Matthias Schmitz,[b] Chris Burdenski,[a] Marcel Baumert,[a] Patrick W. Antoni,[a] Christoph Kerzig,*[b] and Max M. Hansmann*[a]

a) Fakultät für Chemie und Chemische Biologie, Technische Universität Dortmund Otto-Hahn-Str.6, 44227 Dortmund (Germany)
b) Department of Chemistry, Johannes Gutenberg University Mainz, Duesbergweg 10-14, 55128 Mainz (Germany)

Abstract: A new design concept for organic, strongly oxidizing photocatalysts is described based upon dicationic acridinium/carbene hybrids. A highly modular synthesis of such hybrids is presented and the dications are utilized as novel, tailor-made photoredox catalysts in the direct oxidative C−N coupling. Under optimized conditions, benzene and even electron-deficient arenes can be oxidized and coupled with a range of *N*-heterocycles in high to excellent yields with a single low-energy photon per catalytic turnover, while commonly used acridinium photocatalysts are not able to perform the challenging oxidation step. In contrast to traditional photocatalysts, the here reported hybrid photocatalysts feature a reversible two-electron redox system with regular or inverted redox potentials for the two-electron transfer. The different oxidation states could be isolated and structurally characterized supported by NMR, EPR and X-ray analysis. Mechanistic experiments employing time-resolved emission and transient absorption spectroscopy unambiguously reveal the outstanding excited-state oxidation potential of our best-performing catalyst (+2.5 V vs. SCE) and they provide evidence for mechanistic key steps and intermediates.

INTRODUCTION: Photoredox catalysis employing metal-based as well as organic photocatalysts has developed into a modern, powerful toolbox for synthetic organic chemistry.[1] The direct oxidative functionalization of benzene and its derivatives to replace the C−H bond by a C−N bond is a challenging and synthetically highly useful reaction. It represents a short-cut to the widely utilized Buchwald-Hartwig amination which requires pre-functionalized starting materials and transition metal catalysts. Nicewicz and co-workers developed the oxidative amination of electron-rich arenes utilizing acridinium based photocatalysts in combination with oxygen and TEMPO as an additional additive (Scheme 1A).[2] Initially, the transformation was limited to electron-rich arenes such as anisole but was not performed with benzene or electron-deficient derivatives, since the oxidation potentials are too high. To access such high oxidation potentials other concepts are required (Scheme 1B). Wickens and co-workers developed arene azolation reactions using an organic photocatalyst utilizing the consecutive Photoinduced Electron Transfer (conPET) mechanism,[3] which was also exploited by Wagenknecht for challenging oxidations.[4] The method was effective for benzene or methylated arenes, whereas the oxidation of electron-deficient arenes, such as PhCl, produced a low yield of only 22% of the azolated product. An alternative to the conPET process has been recently reported by the Lambert and Barham groups using a photo electrocatalytic approach.[5] However, this method requires specific, additional electrochemical equipment and is technically more complex compared to Nicewicz's arene amination involving a purely photochemical process.[1a,6] Without electrochemical conditions, no products or a very low yield were observed and in general very long reaction times were required. Thus, promoting this transformation using photochemical strategies would be a synthetically convenient addition to existing processes.
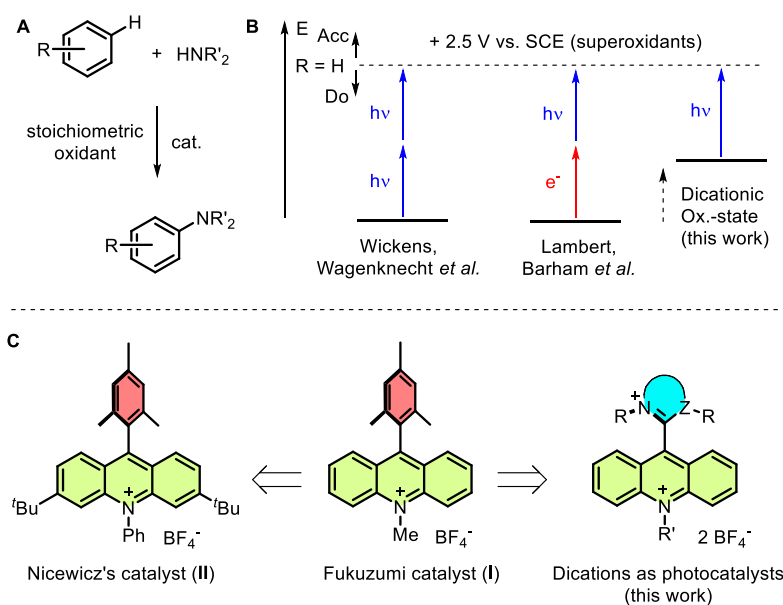

Figure 1. A: Amination by oxidative C−H functionalization. B: Concepts for strongly oxidative photocatalysis. C: Design of acridinium based photocatalysts.

The aim of developing a photocatalyst system that can efficiently oxidize feedstock aromatic compounds like benzene, as well as electron-deficient arenes, through a single photoexcitation remains an exciting challenge. To achieve strongly oxidative redox potentials, new photocatalyst design concepts are highly desired, especially since organic chromophores offer plenty of space for structural design. In contrast to more sophisticated conPET and photo electro chemistry concepts, we envisioned the modification of the well-known Fukuzumi catalyst **I** (Figure 1C).[7] While there have been modifications to the Fukuzumi catalyst,[8] those structural changes typically relate to rather minor changes of the acridinium core in order to increase the photochemical stability (Nicewicz's catalysts **II**).[9] Here, we present a strong modification exchanging the mesityl fragment with a cationic heterocycle. Note, this exchange is not trivial since the mesityl group plays a crucial role in accessing the long-lived charge-transfer Acr$^{\bullet}$-Mes$^{\bullet+}$ state.[7,10] The idea was to access highly electron-deficient catalysts in the ground-state based upon dications thereby raising the ground-state oxidation potential. When excited by a single photon, they should become a powerful photocatalyst for oxidative photocatalysis, bypassing conPET and photo electro mechanisms (Figure 1B). Here we describe the photocatalyst synthesis, application and photochemical characterization including mechanistic studies of a dicationic photocatalyst design.

RESULTS AND DISCUSSION

Design and Characterization of the Photocatalyst Redox-System

To access the desired dicationic acridinium salts, a simple and easily tunable synthetic pathway was envisioned, allowing a rapid synthesis of a diverse set of new chromophores. Inspired by our previous work on pyrylium and pyridinium carbene hybrids,[11] we targeted a carbene addition/deprotonation protocol utilizing *N*-substituted acridinium salts.[8a] Upon addition of IMes carbene[12] to a solution of *N*-Me acridinium **1a**, the addition product **2** could be isolated (Scheme 1). Deprotonation of intermediate **2** with a strong base such as KHMDS or a second equivalent carbene gives rise to the neutral IMes/acridinium hybrid **3a** in 64% yield over two steps. In analogy, the synthesis of the *N*-arylated **3b** or longer *N*-alkyl hybrids **3c** can be performed simply by starting from the corresponding *N*-Ph/*N*-alkyl acridinium salts **1b/1c**. Next, a selection of two stable carbenes featuring a different degree of π-accepting properties, CAAC[13] and DAC[14] were investigated. Both were reacted with *N*-Me as well the *N*-Ph acridinium salts to give the hybrids **4a/4b** and **5a/5b** in good yields of 63−84% in a one-pot strategy. Due to convenience, two equivalents of carbene were utilized in which the second equivalent deprotonates the intermediate **2**, circumventing its isolation. The protonated carbene side product can be easily separated by extraction and reused. Subsequently, the electrochemistry of the new hybrid molecules was investigated by cyclic voltammetry (Figure 2; for **3c** see the SI). While the *N*-Me vs.

N-Ph substitution had rather a minor impact on the relative redox properties (ΔE < 100 mV), a dramatic effect was observed for exchanging the carbene entities.
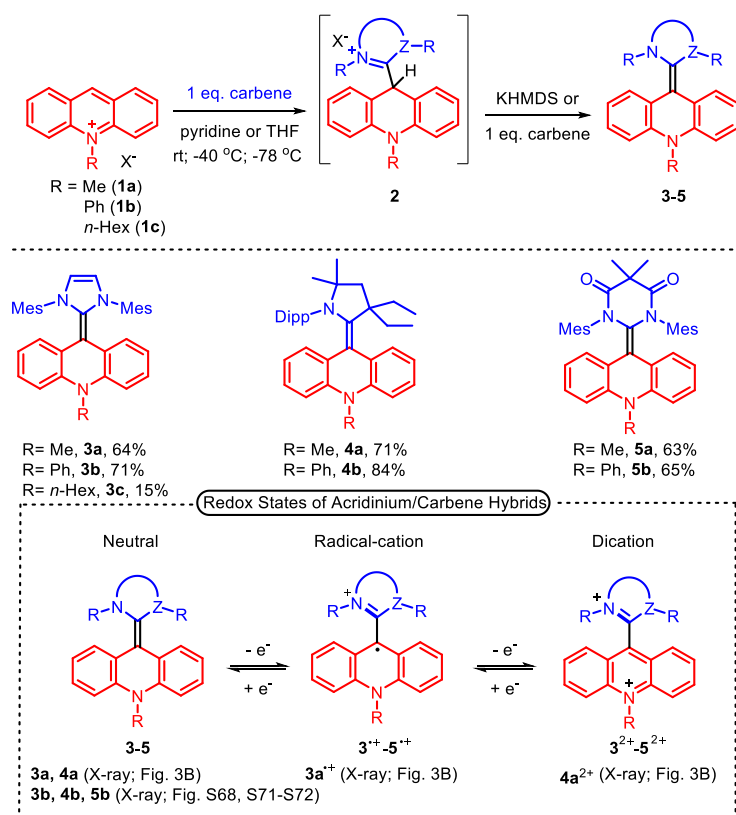
Scheme 1. Synthetic approach towards acridinium/carbene hybrids. X^- = OTf$^-$ or BF$_4^-$.
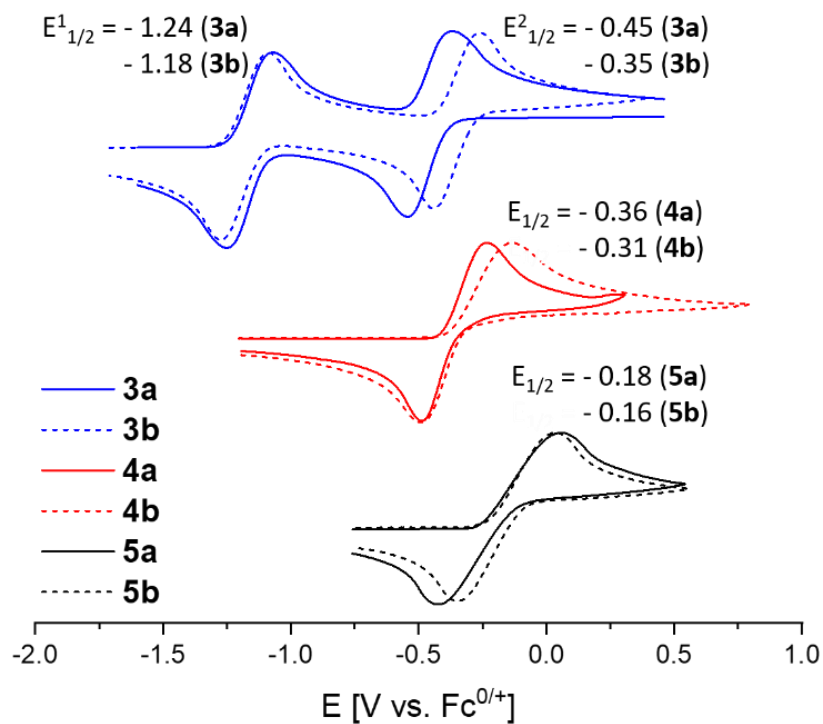

Figure 2. Comparison of cyclic voltammograms (CVs) for the redox systems **3a/3b-5a/5b** in THF (0.1 M *n*-Bu$_4$NPF$_6$) at room temperature; scan rate 200 mV s^{-1}.

In case of IMes hybrid **3a**, two well separated reversible redox-events at $E^1_{1/2}$ = −1.24 V and $E^2_{1/2}$ = −0.45 V (vs. Fc/Fc$^+$) were observed to give the radical cation and dication, respectively. In stark contrast CAAC and DAC hybrids **4a** and **5a** only feature a single two-electron oxidation at −0.36 V and −0.18 V. The general trend of more negative redox potentials for the IMes hybrid is in agreement with the low π-accepting properties as observed for pyrylium and pyridinium hybrids.[11] Note, in those cases no potential compressions/inversions have been observed in which the second electron transfer proceeds at the same redox event. In order to investigate the difference in redox properties, we performed spectroelectrochemical measurements for all systems (Figure 3A). As indicated by the spectroelectrochemistry (SEC) data in the case of IMes hybrid **3a** (for **3b** see Figure S44), the radical cation appears with a very characteristic strongly bathochromic shifted UV-Vis absorption at $\lambda \sim 600$ nm. In case of **4a** and **5a**, only the UV-Vis absorption of the neutral and dicationic oxidation states could be observed in agreement with the CV data. Next, the stoichiometric synthesis of all oxidation states was targeted for the hybrid molecules. Since the CV data of **3a** and **3b** indicated the possibility to generate the radical cations **3a$^{•+}$** and **3b$^{•+}$**, we first attempted their stoichiometric synthesis. Upon addition of one equivalent of AgSbF$_6$ to **3a**, **3a$^{•+}$** SbF$_6^-$ could be isolated as an intensely purple colored solid in 92% yield. In case of neutral **3a** and its radical cation **3a$^{•+}$** we were able to obtain single crystals suitable for X-ray diffraction (Figure 3B). Quite strikingly, neutral **3a** is distorted in a butterfly fashion with a strongly pyramidalized *N*-Me group (sum of angles around N3: 349.1°). In the radical cation **3a$^{•+}$** a major structural reorganization took place in which the imidazolium heterocycle is twisted by 59.1(3)° to the acridinium plane. The simulated EPR spectra of the respective radical cations are in good agreement with the experimentally measured EPR spectra of the monomeric radical cations in solution (Figure 3C; for the EPR of **3b$^{•+}$** and **3c$^{•+}$** see Figures S51-S54). The calculated SOMO shows spin density distributed largely over the acridine heterocycle. Oxidation of **3a** or **3b** with two equivalents of AgSbF$_6$ or AgBF$_4$ cleanly afforded the dications **3a^{2+}/3b^{2+}** as SbF$_6^-$ or BF$_4^-$ salts in high yields (see SI).
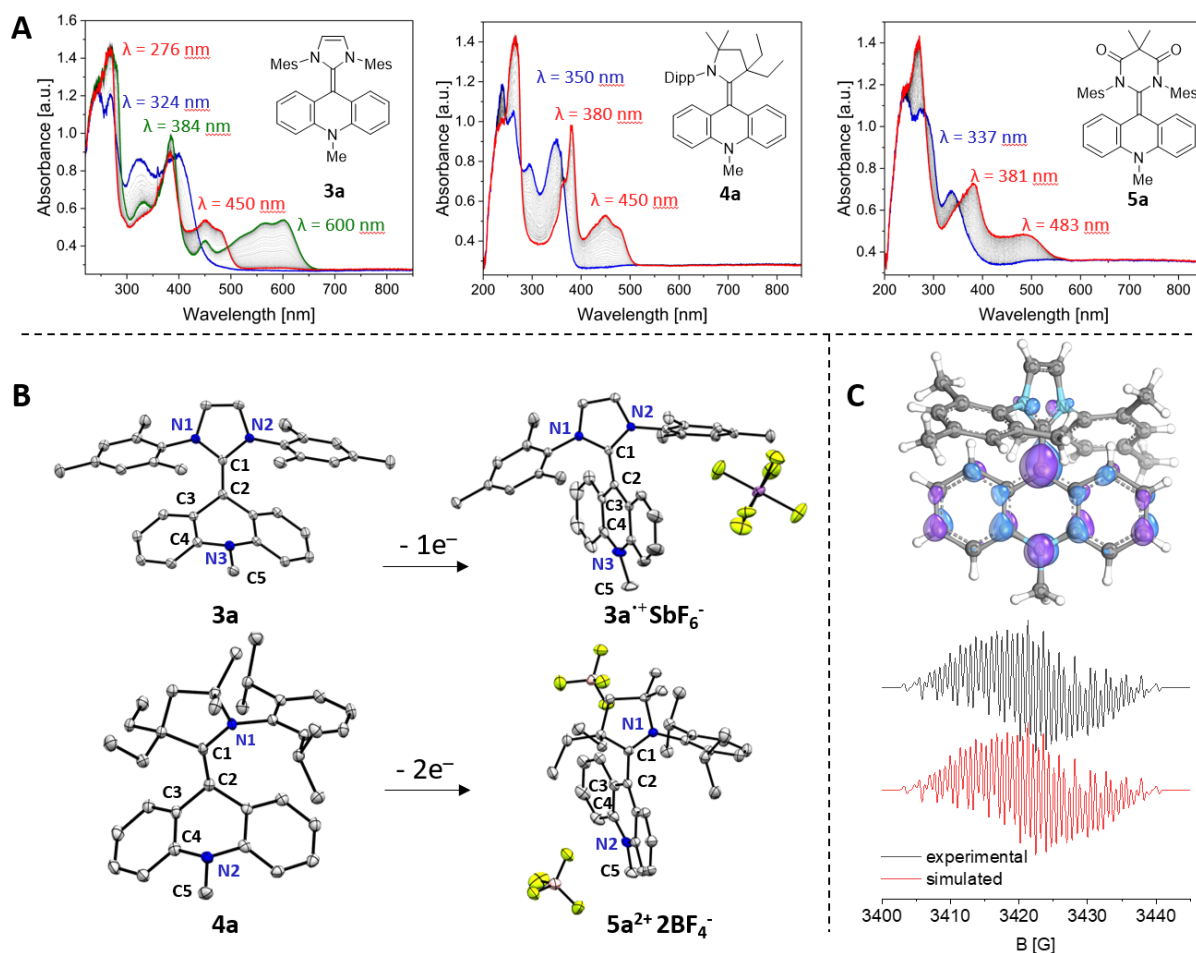
Figure 3. A: Spectroelectrochemistry of hybrids **3a**-**5a**; blue: neutral; green: radical cation; red: dication. B: X-ray solid-state structures of neutral **3a**, radical cation **3a·+** containing the SbF_6^- counter anion, neutral **4a** and dication **4a²⁺** containing the BF_4^- counter anion. Thermal ellipsoids are shown with 50% probability. Hydrogen atoms and solvent molecules (CH_2Cl_2) are omitted for clarity. Selected bond lengths and angles in [Å] and [°]: Top left (**3a**) C1–C2 1.384(4), C2–C3 1.482(3), C3–C4 1.419(4), N3–C5 1.450(4), N1–C1–C2–C3 -3.1(4); Top right (**3a·+**) C1–C2 1.467(3), C2–C3 1.430(3), C3–C4 1.425(3), N3–C5 1.497(7), N1–C1–C2–C3 59.1(3); Bottom left (**4a**) C1–C2 1.360(3), C2–C3 1.496(3), C3–C4 1.416(3), N2–C5 1.450(3), N1–C1–C2–C3 9.9(4); Bottom right (**4a²⁺**) C1–C2 1.505(4), C2–C3 1.430(5), C3–C4 1.441(4), N2–C5 1.383(4), N1–C1–C2–C3 94.8(3). C: Calculated (B3LYP/def2TZVPP//B3LYP-D3BJ/def2SVP) SOMO (isovalue of 0.4); EPR-spectrum of radical cation **3a·+ SbF₆⁻** fitted EPR parameters in [MHz]: 1xN 12.9, 1xN 9.6, 1xN 8.3, 1xH 4.0, 1xH 6.3; 1xH 8.0, 1xH 4.8; 3xH 6.2.

Next, we investigated the oxidation of **4a/4b** and **5a/5b** by two equivalents of silver salts ($AgBF_4/AgSbF_6$). In analogy, all dications **4a²⁺/4b²⁺** as well as **5a²⁺/5b²⁺** could be isolated and characterized. In the ¹H NMR all the acridinium related signals are significantly downfield shifted compared with the neutral compound, which is in line with an increase of aromaticity upon oxidation. In case of the CAAC system **4a**, we were able to obtain single crystals of the neutral and

dicationic oxidation states that were suitable for X-ray diffraction (Figure 3B). Again, a striking large structural reorganization is detected upon oxidation, which agrees with a potential compression/inversion mechanism.[15] The neutral oxidation state is highly distorted in a butterfly shape while in the dication the two heterocyclic planes are oriented in a perpendicular fashion.

Oxidative Photocatalysis by Tailored Photocatalysts – Benzene Oxidation and Beyond

The electron deficient ground state of the dications [E ∼ −0.45 V (**3a²⁺**), −0.36 V (**4a²⁺**), −0.18 V (**5a²⁺**)] is by more than 500 mV positively shifted compared to monocationic Fukuzumi or Nicewicz catalysts (ca. −1.0 V, Figures S38 and S40). This significant increase in the ground-state oxidation potential matches with the outlined motivation of accessing high oxidation potentials upon single photon excitation (Figure 1B). Due to its electron deficiency, we investigated the application of the dications as catalysts in strongly oxidizing photocatalysis. We selected oxidative arene azolation reactions as model transformations. Benzene was selected as the oxidative coupling partner and investigated in a Stern-Volmer experiment (Figure 4).
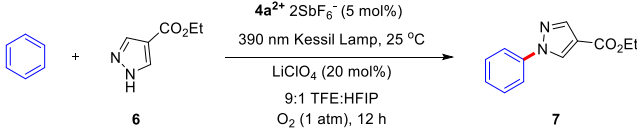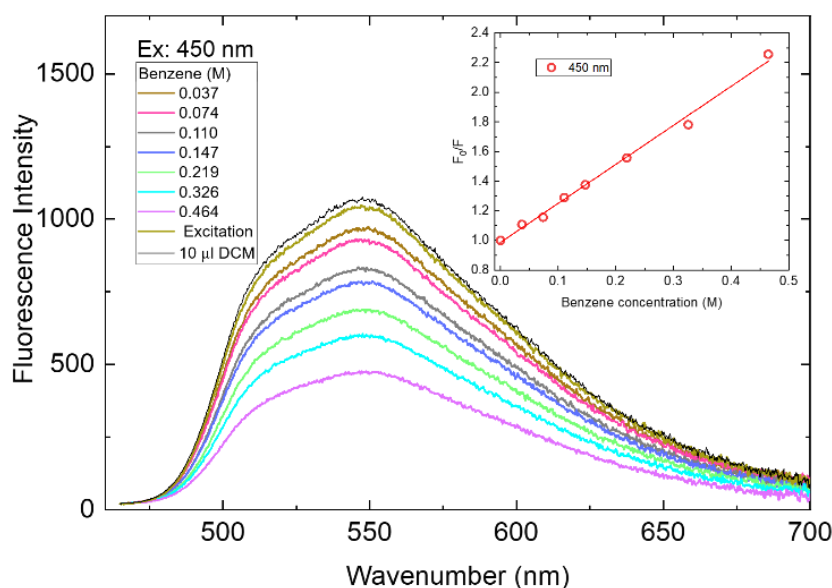

Figure 4. Fluorescence emission spectra and Stern-Volmer plot of **4a²⁺** (0.51 μM) in CH_2Cl_2 with different amounts of benzene.
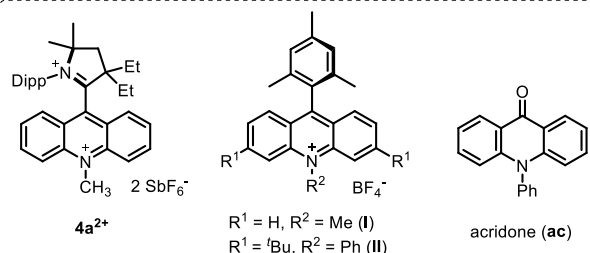
Indeed, we were delighted to observe that the fluorescence signal of dication **4a²⁺** was linearly quenched upon addition of benzene (Figure 4; inset) suggesting the possibility to oxidize benzene [E_{ox}(benzene) ∼ 2.5 V vs. SCE;[3] vide infra]. We then investigated trapping of the benzene radical cation with 1*H*-pyrazole-4-carboxylate (**6**) as a coupling partner under Kessil lamp irradiation (390 nm) employing catalytic amounts (5 mol%) of dication **4a²⁺** and oxygen (1 atm) as stoichiometric oxidant at 25 °C in CH_2Cl_2. To our pleasure, the desired product ethyl 1-phenyl-1*H*-pyrazole-4-carboxylate **7** was obtained in 29% yield after 12 h (Table S3, entry 1, see the Supporting Information). Encouraged by this initial result, a further optimization of the reaction

conditions was performed. Different light sources, solvents, oxidants, light intensity, catalyst loadings, additives, and low-temperature effects were screened (see Table S1–S8, Supporting Information). Gratifyingly, after these optimizations, the yield of the desired azolation product **7** increased to 93% in the presence of 5 mol% catalyst **4a^{2+}** 2SbF$_6^-$, and 20 mol% LiClO$_4$, in a solvent mixture trifluoroethanol (TFE):hexafluoroisopropanol (HFIP) (9:1) under 390 nm blue LED Kessil lamp irradiation for 12 h at 25 °C (Table 1, entry 1).

Table 1. Reaction conditions and control experiments.[a]

| Entry	Deviation from the optimized conditions	Yield of **7**[b] (%)
1	none	93
2	without LiClO$_4$	84
3	under argon	2
4	in dark	0
5	without catalyst	1
6	**I/II** instead of **4a^{2+}**	4/6
7	**ac** instead of **4a^{2+}**	0
8	**3a^{2+}** (5 mol%)	57% (82%)[c]
9	**5a^{2+}** (5 mol%)	51% (81%)[c]
10	440 nm	63

[a]Reactions were performed using 0.4 mmol of pyrazole **6**, benzene (8 mL), catalyst (5 mol%), LiClO$_4$ (20 mol%), solvent mixture TFE:HFIP (9:1) and irradiated with two 390 nm Kessil lamps (40 W) for 12 h providing external water cooled chiller support to maintain the reaction temperature at 25 °C. [b]Yields determined by ^{1}H NMR using mesitylene as an internal standard. [c]Increased reaction time to 24 h.

Previous reports[3,16] motivated us to screen the optimization in the presence of fluorinated solvents which offer higher stability of the involved radical cations. Only a slight reduction in yield (84%) was observed when the reaction was carried out without LiClO$_4$ (Table 1, entry 2). Note, without any additives, Nicewicz and *N*-phenylphenothiazine catalysts failed to activate arenes with a satisfactory yield.[2,3] To confirm if air was required for the photocatalytic reaction, the reaction was carried out under an argon atmosphere. As expected, the desired product **7** did form only in traces (2%) in the absence of air (Table 1, entry 3). No product was formed in the dark confirming a light-mediated transformation (Table 1, entry 4). The requirement of light was additionally verified by light on/off experiments, which showed the constant requirement of

irradiation over 12 h reaction time, disfavoring radical chain reactions (Figure S63). Only trace amounts of the product formed in the absence of the catalyst (Table 1, entry 5). Importantly, under otherwise identical reaction conditions, the substitution of **4a²⁺** by other acridinium-based photocatalysts such as Fukuzumi catalyst (**I**) or Nicewicz catalyst (**II**) resulted in only trace yields of azolation product (Table 1, entries 6-7). Replacement of **4a²⁺** by acridone (**ac**) provided no product, confirming the importance of the cationic heterocycle in the 9-position of the acridinium core. A screening of the three acridinium/carbene hybrids **3a²⁺-5a²⁺** (Table 1, entries 8-9) identified **4a²⁺** to be superior compared to the other dicationic hybrids **3a²⁺** and **5a²⁺** although the catalysts also afforded high yields especially upon prolonged irradiation times for 24 h (Table 1 and Figure S62). Next, under identical conditions, the influence of the *N*-substitution was investigated by using catalysts **4a²⁺** (*N*-Me) and **4b²⁺** (*N*-Ph). We reasoned that *N*-Ph substitution should be superior in its performance since the *N*-Me group could be prone to dealkylation as potential catalyst decomposition pathway. Gratifyingly, both catalysts performed similarly well 93% (**4a²⁺**) and 91% (**4b²⁺**), most likely since with 5 mol% catalyst loading the catalyst decomposition is not yet relevant. In fact, we investigated lowering both catalyst loadings of **4a²⁺** and **4b²⁺** to 0.25 mol% to still obtain slightly reduced yields of 51% and 76% (Table S7). The better performance of the *N*-Ph catalyst at low catalyst loadings agrees with a more robust catalyst system similar to the Fukuzumi/Nicewicz catalyst comparison.[8a,17] That reasoning is further substantiated by an assay comparing the inherent stability of both catalysts upon blue cw laser excitation (Figure S74). Under these conditions, **4b²⁺** is more photostable than **4a²⁺** by almost one order of magnitude.

In order to judge the stability, we investigated catalyst longevity experiments. Three successive catalytic runs by using 5 mol% of catalyst **4a²⁺** were performed (see the SI for details). After three catalytic reactions, the yield of the desired product remained constantly high (90%; Figure S64). This result validates that the catalyst stays active for three consecutive catalytic runs and further encouraged us to check the catalyst's recovery ability after successful catalysis. We also performed a control experiment to check if the catalyst remains intact throughout the catalysis. The catalyst loading was increased to 40 mol% under otherwise identical photocatalysis conditions. ^{1}H NMR in CD_3CN of the reaction mixture showed a clean conversion with an unaltered catalyst structure (Figure S65), indicating good stability in the reaction mixture and disfavoring an assumption in which a decomposition product could be photochemically active. Finally, we also investigated the influence of the catalyst's counter anion,[19a] but noticed no significant influence on the performance employing dicationic catalysts **4a²⁺** with two SbF_6^- (93%) or BF_4^- (88%) counter anions. Additionally, it was tested if we could start the catalysis directly from the neutral oxidation state of the catalyst. Employing neutral **4a**, we only achieved a 25% yield of the desired C−N coupled product, confirming the need for dication-based catalysts (Figure S62).

After extensive optimization and control experiments, the scope of the catalysis was investigated (Scheme 2).
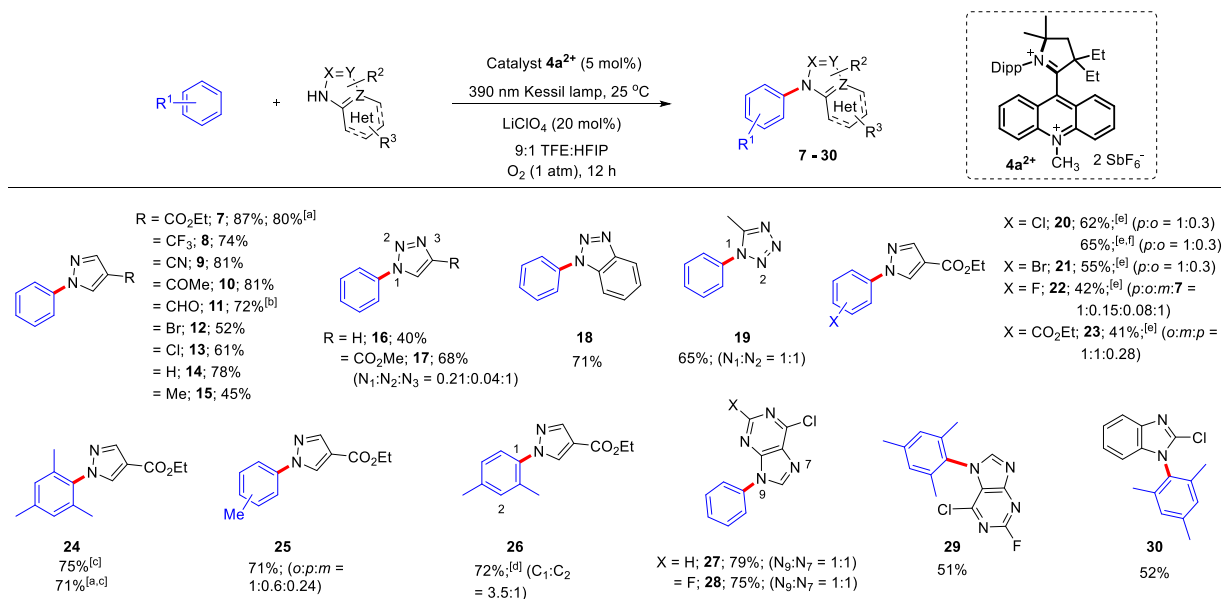
Scheme 2. Substrate scope of arene C−H amination. All isolated yields. Reactions were performed using 0.4 mmol of heterocycle, arene (8 mL), catalyst **4a²⁺** (5 mol%), LiClO₄ (20 mol%), solvent mixture TFE:HFIP (9:1) under irradiation with two 390 nm Kessil lamps for 12 h providing external chiller support to maintain the reaction temperature at 25 °C. [a]Without LiClO₄. [b]1:1 HFIP:PhH solvent. [c]5 eq. arene. [d]10 eq. arene. [e]Reaction time 24 h. [f]Catalyst **4b²⁺**.

Pyrazole derivatives bearing electron-withdrawing moieties such as −CO₂Et, −CF₃, −CN, and −COMe at the C4 position of pyrazole underwent smooth reaction with benzene to deliver the corresponding *N*-Ph pyrazole products (**7**-**10**) in excellent isolated yields (74−87%). We were delighted to discover that even the oxidation-prone carbaldehyde (−CHO) at the C4 position of the pyrazole (**11**, 72%) was well tolerated. Synthetically significant C4-halo substituted pyrazoles (**12**, 52% and **13**, 61%) were also effectively coupled. Parent pyrazole and its derivative featuring electron-donating methyl substitution at the C4 position reacted smoothly with benzene to afford the coupling products **14** (78%) and **15** (45%), respectively. Next, we investigated other *N*-heterocycles than pyrazoles as coupling partners. Unsubstituted 1,2,3-triazole and acceptor substituted 1,2,3-triazole (−CO₂Me) afforded the *N*-phenylated products **16** and **17** ($N_1:N_2:N_3$ = 0.21:0.04:1) in 40% and 68% yields, respectively. Benzotriazole and 5-methyltetrazole were also well suited as a coupling partner to provide the desired products **18** and **19** ($N_1:N_2$ = 1:1) in 71% and 65% isolated yields, respectively. Next, we focused on highly challenging electron-deficient substrates to oxidize. We were delighted to observe that electron-deficient arenes such as chlorobenzene and bromobenzene reacted smoothly with ethyl 1*H*-pyrazole-3-carboxylate to furnish the desired products **20** (*p:o* = 1:0.3) and **21** (*p:o* = 1:0.3) in 62% and 55% yields,

respectively. *N*-Ph catalyst **4b²⁺** provided in case of the oxidation of chlorobenzene slightly improved yields (65%) with the same isomer ratio (*p*:*o* = 1:0.3).

Remarkably, even fluorobenzene could be successfully employed as an arene source to give the desired product **22** in 42% yield as a mixture of isomers in combination with the defluorinated product **7** (*p*:*o*:*m*:**7** = 1:0.15:0.08:1). The catalytic system was even effective to oxidize ethyl benzoate to give **23** in 41% yield as a mixture of isomers (*o*:*m*:*p* = 1:1:0.28). Electron-rich arenes such as mesitylene, toluene, and *m*-xylene afforded the corresponding pyrazole coupling products **24** (75%), **25** (71%, *o*:*p*:*m* = 1:0.6:0.24 and **26** (72%, C_1:C_2 = 3.5:1) in high yields, respectively. Finally, we investigated more complex heterocycles and selected halogenated purines as coupling partners. In this case, both the coupling with benzene or mesitylene resulted in the isolation of **27** (79%, N_9:N_7 = 1:1), **28** (75%, N_9:N_7 = 1:1) and **29** (51%) in good yields.

In our reaction protocol, we discovered that *N*-heterocyclic nucleophiles such as 2-chlorobenzimidazole can be directly coupled to an arene such as mesitylene, resulting in a yield of 52% of **30**. When the catalytic activity was checked without any additional additives, we found that our catalytic system can even deliver nearly the same yield without any additional additives such as $LiClO_4$. The coupling between benzene and 1*H*-pyrazole-4-carboxylate provides **7** with 87% and 80% yield with and without $LiClO_4$ respectively. Additionally, the coupling of mesitylene and 1*H*-pyrazole-4-carboxylate provides 75% and 71% yield of **24** with and without $LiClO_4$ respectively.

Mechanistic Investigations

Evidently, **4a²⁺** and **4b²⁺** are potent catalysts for oxidative C−N coupling reactions with challenging substrates. Initial mechanistic irradiation experiments with different output power settings of the LEDs and shorter reaction time (5 h, to avoid saturation effects, Table S6) did not show a pronounced power-dependence, indicating a one-photon mechanism.[18] However, the results presented so far do not provide clear mechanistic insights, in particular as (i) the radical cations **4a•⁺/4b•⁺** could not be characterized (spectro)electro-chemically and (ii) the role of O_2 in the mechanism has to be clarified. First, we had a closer look at the properties of the emissive excited singlet states of **4a²⁺/4b²⁺**. The excited-state energies E_{00} are on the order of 2.5 eV and very similar for both compounds (Figure 5). The excited states decay monoexponentially with a typical lifetime of a few nanoseconds. That lifetime is shorter in MeCN compared to CH_2Cl_2 by a factor of ~3 and we observed a dependence on the counteranion in the latter solvent (see Table S12 for details and the discussion below).[19] Importantly, there is essentially no quenching of excited **4a²⁺** or **4b²⁺** by dissolved oxygen (inset Figure 5 and Table S12-14), which was an important mechanistic step in a recent study on light-induced benzene oxidation.[3]

In contrast to what has been observed for some acridinium[8b] and structurally related isoacridone[20] dyes, we did not observe any long-lived signals in the transient absorption (TA) spectra recorded upon direct excitation of **4a²⁺/4b²⁺** (regardless of the counteranion and the solvent), allowing us to exclude triplet formation. The absence of triplet states likely contributes to the outstanding robustness of this new photocatalyst class.
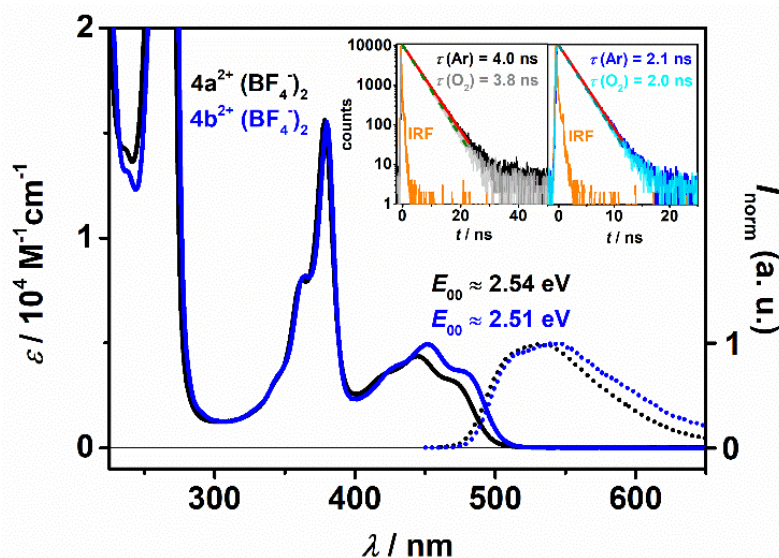

Figure 5. Calibrated UV-Vis absorption spectra and normalized emission spectra of **4a²⁺/4b²⁺** in MeCN, along with the E_{00} determination. Inset: Excited-state lifetime upon 446 nm excitation in Ar- and O_2- saturated solution.

As the two-electron oxidation/reduction potential (Figure 2) seems inappropriate for the determination of the required potential for the **4a²⁺/4a·⁺** couple and the excited-state reduction potential $E(*\textbf{4a}^{2+}/\textbf{4a}^{·+})$ accordingly,[21] we carried out a detailed Rehm-Weller[22] analysis to obtain that quantity. For that, we carried out time-resolved quenching experiments with nine different benzene and biphenyl derivatives and analyzed the resulting quenching rate constants as a function of the oxidation potential of the quencher (Figure 6 and Figure S79). These studies were carried out in MeCN because reliable quencher oxidation potentials, which are crucial for this analysis, are available in this solvent.[23] In line with the expected quenching through the transfer of a single electron from the quencher to the excited catalyst, the bimolecular rate constants decrease with increasing oxidation potentials of the former. The $E(*\textbf{4a}^{2+}/\textbf{4a}^{·+})$ resulting from a fit based on the Rehm-Weller model is as high as +2.52 V vs. SCE (corresponding to +2.14 V vs. Fc/Fc⁺).[24] Subtracting E_{00} from that quantity yields $E(\textbf{4a}^{2+}/\textbf{4a}^{·+})$= -0.02 V vs. SCE (-0.40 V vs. Fc/Fc⁺) for the reduction potential of **4a²⁺**, which is extremely close to the value obtained for the two-electron reduction (-0.36 V vs. Fc/Fc⁺).
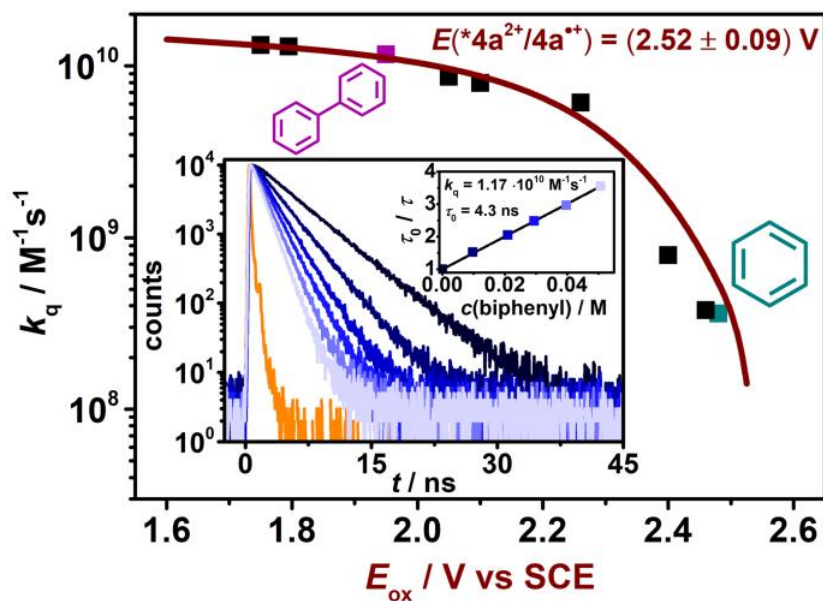
Figure 6. Kinetic determination of the excited-state reduction potential of **4a²⁺** with various benzene and biphenyl derivatives in acetonitrile. Inset: TCSPC measurements of lifetime reduction of ***4a²⁺** with increasing biphenyl (BP) concentration and the corresponding Stern–Volmer plot as an example. See SI for details.

The excited-state reduction potential of **4a²⁺** compares favorably with that of most known photocatalysts[9b,16a,25] and it seems that only the 3-cyano-1-methylquinolinium ion, which does not absorb visible light, is a significantly stronger photooxidant.[26] Moreover, the oxidative power of **4a²⁺** is comparable to what is obtained with two-photon excitation schemes[3,4,27] or via photoelectrochemistry[5b,5d,28] systems as motivated in the introduction (Figure 1).

For our initial substrate, benzene, several Stern–Volmer quenching studies were carried out (Table S16) using different solvents (CH$_2$Cl$_2$ and MeCN), **4a²⁺** as well as **4b²⁺** and both counter anions (SbF$_6^-$ or BF$_4^-$). All quenching rate constants k_q so obtained are in the range from 1.5 to 5.0 × 10⁸ M⁻¹ s⁻¹, i.e. slightly below the diffusion limit. Under all conditions investigated, the excited *N*-Ph-derivative **4b²⁺** has a shorter lifetime than the *N*-Me-derivative **4a²⁺**, but this is usually compensated by a faster k_q for **4b²⁺** such that the overall quenching efficiencies are comparable for both catalysts. An extrapolation of these results to the actual irradiation conditions (5.6 M of benzene) gives quenching efficiencies on the order of 90%, which implies high quantum yields for the overall reaction and short irradiation times. Nanosecond laser flash photolysis (LFP) studies upon 355 nm excitation of **4a²⁺** in the presence of benzene concentrations allowing up to 90% ***4a²⁺** quenching were carried out to detect both quenching products. However, we only observed baseline-like spectra without any evidence for the benzene radical cation[26] and **4a•⁺**, despite the high sensitivity of our LFP setup.[29] Unproductive and ultrafast back-electron transfer in the so-called solvent cage is spin-allowed for this reaction, which can be regarded as a general problem

for photoinduced electron transfer reactions with photoexcited singlet states.[30] In this particular case, the quantum yield for productive cage escape[31] to yield radical ions that can be detected and intercepted seems to be very low (< 5%).

To obtain clear spectroscopic evidence for substrate oxidation via single-electron transfer, we tested biphenyl BP (which was among the quenchers in Figure 6) because the corresponding radical cation absorbs more strongly,[23a] facilitating its detection even at very low concentrations. Upon selective 355 nm excitation of **4a²⁺** and efficient quenching by BP, we unambiguously identified BP•⁺ in the TA spectra through its characteristic absorption band in the red spectral region (lower part of Figure 7). A spectral separation with the literature-known BP•⁺ spectrum[23a] clearly indicates that the quenching by-product, **4a•⁺**, has an absorption band between 500 and 650 nm. The observed ground-state bleach (GSB) between ~410 and ~480 nm reveals that **4a²⁺** absorbs more strongly than **4a•⁺** in this wavelength range. However, the overall TA intensities are low, likely as a result of inefficient cage escape. Given that (i) the ground state of neutral **4a** does not absorb above 400 nm and (ii) triplet photoreactions typically proceed with higher quantum yields than singlet reactions, we were looking for a suitable triplet chromophore to obtain a reliable spectrum of **4a•⁺** in the visible range via reductive quenching upon selective excitation of the triplet sensitizer.

The excitation of $[Ru(bpy)_3]^{2+}$, which is a sufficiently strong photooxidant for the desired reaction, with 532 nm in the presence of **4a** gave the expected post-quenching spectra with a superposition of $[Ru(bpy)_3]^{•+}$ and **4a•⁺** (upper part of Figure 7). The sensitizer-derived photoproduct (gray spectrum in Figure 7) with a well-known TA spectrum showing an absorption band peaking at ~510 nm and a characteristic ground-state bleach at ~440 nm[31c,32] decays on a microsecond timescale. The remaining TA signals are attributed to the quenching by-product **4a•⁺**. This assignment is based on (i) the similarity to the UV-Vis spectrum of **3a•⁺** (Figure 3A), (ii) our successful spectral separation displayed in the upper part of Figure 7 and (iii) additional kinetic TA measurements (Figure S82). Taking the known difference molar absorption coefficient for $[Ru(bpy)_3]^{•+}$ at 500 nm (~12000 M⁻¹ cm⁻¹),[33] where **4a•⁺** is essentially transparent, the **4a•⁺** spectrum can be calibrated. The calibrated absorption spectra of the hybrid **4a** and its oxidation states are shown in Figure 7 (middle). While **4a•⁺** is inaccessible by electrochemical oxidation/reduction, our investigations clearly demonstrated its photochemical generation from both **4a** and **4a²⁺**, also via a challenging arene oxidation with the singlet-excited state of the latter species. However, the difficulties in obtaining high concentrations of **4a•⁺** under conditions similar to those used for catalysis hamper further meaningful spectroscopic investigations. We, therefore, performed mechanistic irradiation experiments to obtain (indirect) evidence for the **4a²⁺** regeneration in the catalytic cycle under study.
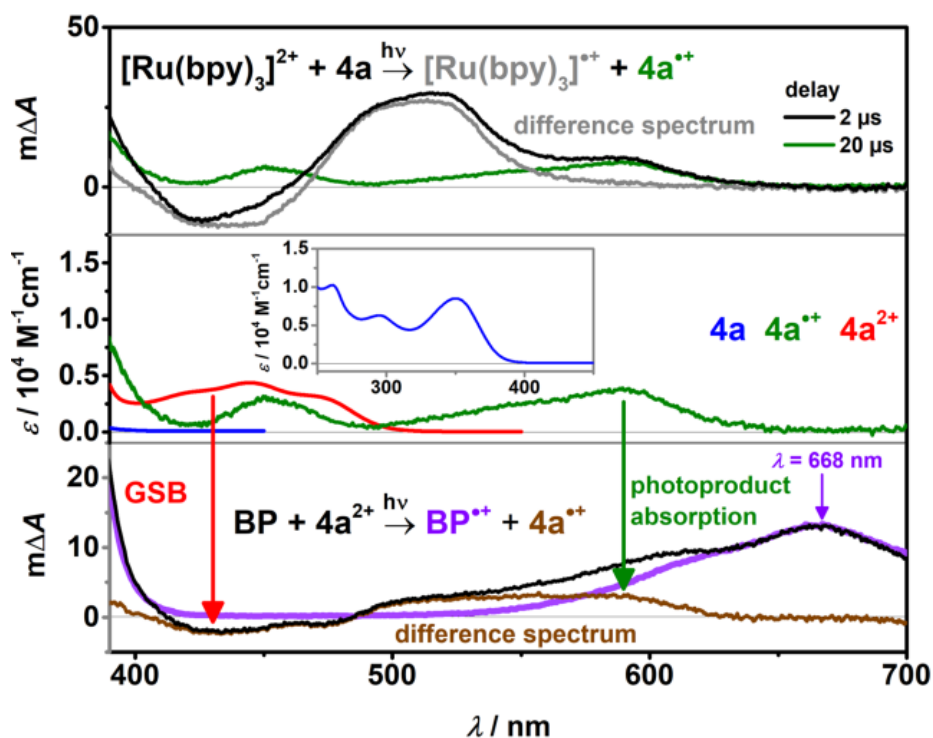
Figure 7. Determination of the spectroscopic signatures of **4a•+**. Top: Transient absorption spectra of a solution containing [Ru(bpy)₃]²⁺ (30 μM) and **4a** (300 μM) in Ar-saturated acetonitrile after laser excitation (532 nm, 5 ns pulse duration) recorded at different delay times. ³[Ru(bpy)₃]²⁺ quenching efficiency under selected conditions, 60%. Middle: UV-Vis spectra of **4a**, **4a•+** and **4a²⁺** in acetonitrile. Bottom: Transient absorption spectra of a solution containing **4a²⁺** (35 μM) and biphenyl (BP, 200 mM) in Ar-saturated acetonitrile after laser excitation (355 nm, delay: 50 ns) as well as a BP•+ reference spectrum[23a] (violet) and the resulting difference spectrum (brown).

Irradiation of an Ar-saturated solution of **4a²⁺** with a green LED in the presence of a high benzene concentration leads to rapid catalyst decomposition, most likely via **4a•+**, given that the catalyst is completely stable in the absence of the quencher benzene (Figure 8A/B). However, **4a²⁺** is almost photostable when the solution is additionally saturated with oxygen, suggesting that an electron transfer with **4a•+** regenerates **4a²⁺**. Related catalyst regeneration steps starting from acridinium radicals were observed previously.[2,34] LiClO₄ slightly improves the stability of **4a²⁺** under our conditions, but O₂ clearly has a more pronounced effect. Similar observations were made during NMR-scale irradiation experiments (see above). In addition to the catalyst regeneration step, O₂ is assumed to facilitate the formal hydrogen atom elimination being required for the formation of the stable C−N coupling product (Figure 8C).[2,35] This reasoning is in agreement with the above-mentioned NMR-scale experiments, which only gave traces of the desired azolation product **7**.
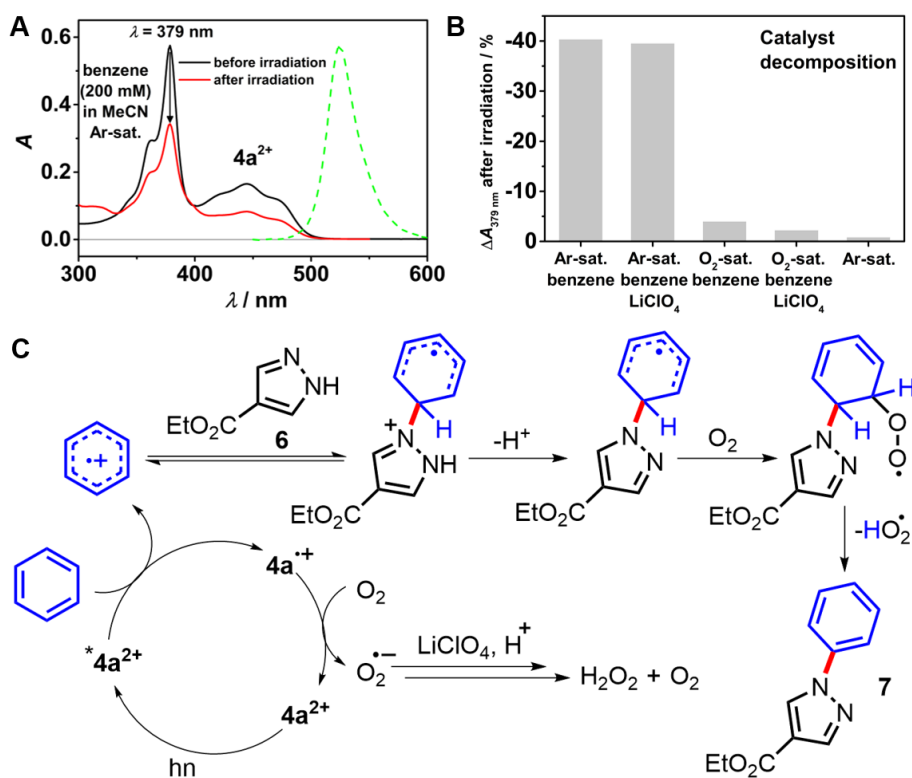
Figure 8. A: UV-Vis spectra of Ar-saturated solutions of **4a²⁺** in acetonitrile in the presence of benzene (200 mM) before and after 5 minutes of irradiation (525 nm, dotted line: emission spectrum of the LED). B: Light-induced decrease of the absorption band of **4a²⁺** in percent at 379 nm in the presence or absence of oxygen and/or LiClO₄ (20 mol%). C: Proposed mechanism for the C–N coupling reactions. The effect of LiClO₄ is described in Ref. 3.

Taking into account all experiments presented herein and the findings from prior studies on this reaction class with highly oxidizing catalytic systems,[2,3] the mechanism can be summarized as displayed in Figure 8C. Interestingly, neither multi-photon nor electrochemical strategies are required for the formation of the arene radical cation. This straightforward and versatile monophotonic C–N coupling approach was enabled through the development of novel hybrid catalysts.

CONCLUSIONS

In summary, we report on the design of novel strongly oxidizing photocatalysts based on dicationic chromophors. The dications were rapidly assembled by a building block approach from stable carbenes and acridinium salts followed by two-electron oxidation. In contrast to typical organic photocatalysts such as Fukuzumi or Nicewicz catalyst, the here described hybrids feature three or two stable redox states depending on the carbene moiety chosen. We show by X-ray diffraction that upon oxidation, a large structural reorganization takes place which agrees with a potential compression/inversion mechanism in the CV. We subsequently applied the dicationic hybrids as

photocatalysts in the oxidative C−N coupling with *N*-heterocycles. Extensive optimization, control experiments as well as a large substrate scope containing even electron deficient arene coupling partners, which are not possible to activate with traditional acridinium photocatalysts, clearly underline the importance of the tailored hybrid photocatalysts. The combination of time-resolved spectroscopic techniques with preparative and mechanistic irradiation experiments provided a clear mechanistic picture and revealed the outstanding excited-state redox potential (E ~ +2.5 V vs. SCE) as well as the excellent photostability of the novel photocatalyst. Excitingly, transient absorption spectroscopy even allowed the UV-Vis identification of the radical cation oxidation state which is not accessible by CV or spectroelectrochemical studies.

Considering the large amount of available carbenes as well as substituted acridinium salts, this work just opens up a large structural space of readily accessible photocatalysts. Especially the design of dicationic and thus intrinsically electron-deficient photocatalysts is yet unexplored and should be applicable to other chromophore cores. Additionally, photocatalysts with inverted redox potentials have been largely overlooked. We are currently investigating novel applications for such strong oxidative photocatalysts and try to deepen our mechanistic understanding by utilizing multi-electron redox systems as photocatalysts.

ACKNOWLEDGMENTS

REFERENCES

[1] (a) Romero, N. A.; Nicewicz, D. A. Organic Photoredox Catalysis. *Chem. Rev.* **2016**, *116*, 10075–10166. (b) Bell, J. D.; Murphy, J. A. Recent advances in visible light-activated radical coupling reactions triggered by (i) ruthenium, (ii) iridium and (iii) organic photoredox agents. *Chem. Soc. Rev.* **2021**, *50*, 9540–9685. (c) Shaw, M. H.; Twilton, J.; MacMillan, D. W. C. Photoredox Catalysis in Organic Chemistry. *J. Org. Chem.* **2016**, *81*, 6898–6926.; (d) Speckmeier, E.; Fischer, T. G.; Zeitler, K. A Toolbox Approach To Construct Broadly Applicable Metal-Free Catalysts for Photoredox Chemistry: Deliberate Tuning of Redox Potentials and Importance of Halogens in Donor−AcceptorCyanoarenes. *J. Am. Chem. Soc.* **2018**, *140*, 15353–15365. (e) Marzo, L.; Pagire, S. K.; Reiser, O.; König, B.; Visible-Light Photocatalysis: Does It Make a Difference in Organic Synthesis?. *Angew. Chem., Int. Ed.* **2018**, *57*, 10034– 10072. (f) Skubi, K. L.; Blum, T. R.; Yoon, T. P. Dual Catalysis Strategies in Photochemical Synthesis. *Chem. Rev.* **2016**, *116*, 10035–10074.
[2] Romero, N. A.; Margrey, K. A.; Tay, N. E.; Nicewicz, D. A. Site-selective arene C-H amination via photoredox catalysis. *Science* **2015**, *349*, 1326–1330.
[3] Targos, K.; Williams, O. P.; Wickens, Z. K. Unveiling Potent Photooxidation Behavior of Catalytic Photoreductants. *J. Am. Chem. Soc.* **2021**, *143*, 4125–4132.
[4] Rombach, D.; Wagenknecht, H.-A. Photoredox Catalytic α-Alkoxypentafluorosulfanylation of α-Methyl- and α-Phenylstyrene Using SF_6. *Angew. Chem., Int. Ed.* **2020**, *59*, 300–303.

[5] (a) Huang, H.; Lambert, T. H. Electrophotocatalytic Acetoxyhydroxylation of Aryl Olefins. *J. Am. Chem. Soc.* **2021**, *143*, 7247–7252; (b) Huang, H.; Strater, Z. M.; Rauch, M.; Shee, J.; Sisto, T. J.; Nuckolls, C.; Lambert, T. H. Electrophotocatalysis with a Trisaminocyclopropenium Radical Dication. *Angew. Chem., Int. Ed.* **2019**, *58*, 13318–13322. (c) Wilson, R. M.; Lambert, T. H. CyclopropeniumIons in Catalysis. *Acc. Chem. Res.* **2022**, *55,* 3057–3069. (d) Žurauskas, J.; Boháčová, S.; Wu, S.; Butera, V.; Schmid, S.; Domański, M.; Slanina, T.; Barham, J. P. Electron-Poor Acridones and Acridiniums as Super Photooxidants in Molecular Photoelectrochemistry by Unusual Mechanisms. *Angew. Chem., Int. Ed.* **2023**, *62*, e202307550. (e) Wu, S.; Kaur, J.; Karl, T. A.; Tian, X.; Barham, J. P. Synthetic Molecular Photoelectrochemistry: New Frontiers in Synthetic Applications, Mechanistic Insights and Scalability. *Angew. Chem., Int. Ed.* **2022**, *61*, e202107811.
[6] Wu, S.; Žurauskas, J.; Domański, M.; Hitzfeld, P. S.; Butera, V.; Scott, D. J.; Rehbein, J.; Kumar, A.; Thyrhaug, E.; Hauer, J.; Barham, J. P. Hole-mediated photoredox catalysis: tris(p-substituted) biarylaminium radical cations as tunable, precomplexing and potent photooxidants. *Org. Chem. Front.* **2021**, *8*, 1132–1142.
[7] S. Fukuzumi, H. Kotani, K. Ohkubo, S. Ogo, N. V. Tkachenko and H. Lemmetyinen, Electron-Transfer State of 9-Mesityl-10-methylacridinium Ion with a Much Longer Lifetime and Higher Energy Than That of the Natural Photosynthetic Reaction Center. *J. Am. Chem. Soc.* **2004**, *126*, 1600–1601.
[8] (a) Tlili, A.; Lakhdar, S. Acridinium Salts and Cyanoarenes as Powerful Photocatalysts: Opportunities in Organic Synthesis. *Angew. Chem., Int. Ed.* **2021**, *60*, 19526–19549. (b) Fischer, C.; Kerzig, C.; Zilate, B.; Wenger, O. S.; Sparr, C. Modulation of Acridinium Organophotoredox Catalysts Guided by Photophysical Studies. *ACS Catal.* **2020**, *10*, 210–215. (c) Zilate, B.; Fischer, C.; Sparr, C. Design and application of aminoacridinium organophotoredox catalysts. *Chem. Commun.* **2020**, *56*, 1767–1775. (d) Cao, Y.-X.; Zhu, G.; Li, Y.; Breton, N. L.; Gourlaouen, C.; Choua, S.; Boixel, J.; Henri-Pierre Jacquot de Rouville, H.-P. J. d.; Soulé, J-F. Photoinduced Arylation of Acridinium Salts: Tunable Photoredox Catalysts for C–O Bond Cleavage. *J. Am. Chem. Soc.* **2022**, *144*, 5902–5909. (e) Hamilton, D. S.; Nicewicz, D. A. Direct Catalytic Anti-Markovnikov Hydroetherification of Alkenols. *J. Am. Chem. Soc.* **2012**, *134*, 18577–18580. (f) A. Gini, M. Uygur, T. Rigotti, J. Alemán, O. García Mancheño, *Chem. Eur. J.* **2018**, 24, 12509–12514. (g) A. Gini, T. Rigotti, R. Pérez-Ruiz, M. Uygur, R. Mas-Ballesté, I. Corral, L. Martínez-Fernández, V. A. de la Peña O'Shea, O. García Mancheño, J. Alemán, *ChemPhotChem* **2019**, *3*, 609-612. (h) K. A. Browne, D. D. Deheyn, G. A. El-Hiti, K. Smith, I. Weeks, *J. Am. Chem. Soc.* **2011**, *133*, 14637–14648. (i) L. Chen, L. Hi. P. Li, L. Wang, *Org. Lett.* **2016**, *18*, 3646–3649.
[9] (a) Joshi-Pangu, A.; Lévesque, F.; Roth, H. G.; Oliver, S. F.; Campeau, L.-C.; Nicewicz, D.; DiRocco, D. A. Acridinium-Based Photocatalysts: A Sustainable Option in Photoredox Catalysis. *J. Org. Chem.* **2016**, *81*, 7244–7249. (b) White, A. R.; Wang, L.; Nicewicz, D. A. Synthesis and Characterization of Acridinium Dyes for Photoredox Catalysis. *Synlett* **2019**, *30*, 827–832.
[10] Fukuzumi, S.; Ohkubo, K. Organic synthetic transformations using organic dyes as photoredox catalysts. *Org. Biomol. Chem.* **2014**, *12*, 6059–6071.
[11] (a) Antoni, P. W.; Hansmann, M. M. Pyrylenes: A New Class of Tunable, Redox-Switchable, Photoexcitable Pyrylium–Carbene Hybrids with Three Stable Redox-States. *J. Am. Chem. Soc.* **2018**, *140*, 14823–14835. (b) Antoni, P. W.; Bruckhoff, T.; Hansmann, M. M. Organic Redox Systems Based on Pyridinium–Carbene Hybrids. *J. Am. Chem. Soc.* **2019**, *141*, 9701–9711. (c) Antoni, P. W.; Golz, C.; Hansmann, M. M. Organic Four-Electron Redox Systems Based on Bipyridine and Phenanthroline Carbene Architectures *Angew. Chem., Int. Ed.* **2022**, *61*, e202203064.
[12] Arduengo III, A. J.; Dias, H. V. R.; Harlow, R. L.; Kline, M. Electronic stabilization of nucleophilic carbenes. *J. Am. Chem. Soc.* **1992**, *114*, 5530–5534.
[13] Lavallo, V.; Canac, Y.; Präsang, C.; Donnadieu, B.; Bertrand, G. *Stable Cyclic (Alkyl)(Amino)Carbenes as Rigid or Flexible, Bulky, Electron-Rich Ligands for Transition-Metal Catalysts: A Quaternary Carbon Atom Makes the Difference*. *Angew. Chem., Int. Ed.* **2005**, *44*, 5705–5709.
[14] Hudnall, T. W.; Bielawski, C. W. An N, N′-Diamidocarbene: Studies in C–H Insertion, Reversible Carbonylation, and Transition-Metal Coordination Chemistry. *J. Am. Chem. Soc.* **2009**, *131*, 16039–16041.
[15] Evans, D. H. One-Electron and Two-Electron Transfers in Electrochemistry and Homogeneous Solution Reactions. *Chem. Rev.* **2008**, *108*, 2113–2144.
[16] (a) Pistritto, V. A.; Schutzbach-Horton, M. E.; David A. Nicewicz, D. A. Nucleophilic Aromatic Substitution of Unactivated Fluoroarenes Enabled by Organic Photoredox Catalysis. *J. Am. Chem. Soc.* **2020**, *142*, 17187–17194. (b) Zhang, L.; Liardet, L.; Luo, J.; Ren, D.; Grätzel, M.; Hu, X. Photoelectrocatalytic Arene C-H Amination. *Nat. Catal.* **2019**, *2*, 366–373. (c) Colomer, I.; Chamberlain, A. E. R.; Haughey, M. B.; Donohoe, T. J. Hexafluoroisopropanol as a Highly Versatile Solvent. *Nat. Rev. Chem.* **2017**, *1*, 1–12.
[17] Gesmundo, N. J.; Grandjean, J-M. M.; Nicewicz, D. A. Amide and Amine Nucleophiles in Polar Radical Crossover Cycloadditions: Synthesis of γ-Lactams and Pyrrolidines. *Org. Lett.* **2015**, *17*, 1316–1319.
[18] Glaser, F.; Kerzig, C.; Wenger, O. S. Multi-Photon Excitation in Photoredox Catalysis: Concepts, Applications, Methods. *Angew. Chem., Int. Ed.* 2020, *59*, 10266–10284.
[19] (a) Farney, E. P.; Chapman, S. J.; Swords, W. B.; Torelli, M. D.; Hamers, R. J.; Yoon, T. P. Discovery and Elucidation of Counteranion Dependence in Photoredox Catalysis. *J. Am. Chem. Soc.* **2019**, *141*, 6385–6391. (b) Earley, J. D.; A. Zieleniewska, A.; Ripberger, H. H.; Shin, N. Y.; Lazorski, M. S.; Mast, Z. J.; Sayre, H. J.; McCusker, J. K.; Scholes, G. D.; Knowles, R. R.; Reid, O. G.; Rumbles, G. Ion-pair reorganization regulates reactivity in photoredox catalysts. *Nat. Chem.* **2022**, *14*, 746–753.
[20] Pfund, B.; Hutskalova, V.; Sparr, C.; Wenger, O. S. Isoacridone dyes with parallel reactivity from both singlet and triplet excited states for biphotonic catalysis and upconversion. ***Chem. Sci.*** **2023**, *14*, 11180–11191.

[21] Boixel, J.; Blart, E.; Pellegrin, Y.; Odobel, F.; Perin, N.; Chiorboli, C.; Fracasso, S.; Ravaglia, M.; Scandola, F. Hole-Transfer Dyads and Triads Based on Perylene Monoimide, Quaterthiophene, and Extended Tetrathiafulvalene. *Chem. Eur. J.* **2010**, *16*, 9140–9153.

[22] (a) Rehm, D.; Weller, A. Kinetics of Fluorescence Quenching by Electron and H-Atom Transfer. *Israel J. Chem.* **1970**, *8*, 259–27l. (b) Farid, S.; Dinnocenzo, J. P.; Merkel, P. B.; Young, R. H.; Shukla, D.; Guirado, G. Reexamination of the RehmWeller Data Set Reveals ElectronTransfer Quenching That Follows a SandrosBoltzmannDependence on Free Energy. *J. Am. Chem. Soc.* **2011**, *133*, 11580–11587. (c) Zeman, C. J.; Kim, S.; Zhang, F.; Schanze, K. S. Direct Observation of the Reduction of Aryl Halides by a Photoexcited Perylene Diimide Radical Anion. *J. Am. Chem. Soc.* **2020**, *142*, 5, 2204–2207.

[23] (a) Merkel, P. B.; Luo, P.; Dinnocenzo, J. P.; Farid, S. Accurate Oxidation Potentials of Benzene and Biphenyl Derivatives via Electron-Transfer Equilibria and Transient Kinetics. *J. Org. Chem.* **2009**, *74*, 5163–5173. (b) Huang, H.; Lambert, T. H. Electrophotocatalytic SNAr Reactions of Unactivated Aryl Fluorides at Ambient Temperature and Without Base. *Angew. Chem., Int. Ed.* **2020**, *59*, 658–662.

[24] Pavlishchuk, V. V.; Addison, A. W. Conversion constants for redox potentials measured versus different reference electrodes in acetonitrile solutions at 25°C. *Inorg. Chim. Acta* **2000**, *298*, 97–102.

[25] (a) Wu, X.; Chen, W.; Holmberg-Douglas, N.; Bida, G. T.; Tu, X.; Ma, X.; Wu, Z.; Nicewicz, D. A.; Li. Z. ^{11}C-, ^{12}C-, and ^{13}C-cyanation of electron-rich arenes via organic photoredox catalysis. *Chem* **2023**, *9*, 343–362. (b) Schlegel, M.; Qian, S.; Nicewicz, D. A. Aliphatic C−H Functionalization Using Pyridine *N*-Oxides as H-Atom Abstraction Agents. *ACS Catal.* **2022**, *12*, 10499–10505. (c) Pistritto, V. A.; Liu, S.; Nicewicz, D. A. Mechanistic Investigations into Amination of Unactivated Arenes via Cation Radical Accelerated Nucleophilic Aromatic Substitution. *J. Am. Chem. Soc.* **2022**, *144*, 15118–15131. (d) Bertrams, M-S.; Hermainski, K.; Mörsdorf, J-M.; Ballmann, J.; Kerzig, C. Triplet quenching pathway control with molecular dyads enables the identification of a highly oxidizing annihilator class. *Chem. Sci.* **2023**, *14*, 8583–8591. (e) Fukuzumi, S.; Ohkubo, K. Selective photocatalytic reactions with organic photocatalysts. *Chem. Sci.* **2013**, *4*, 561–574. (f) Romero, N. A.; Nicewicz, D. A. Mechanistic Insight into the Photoredox Catalysis of Anti-Markovnikov Alkene Hydrofunctionalization Reactions. *J. Am. Chem. Soc.* **2014**, *136*, 17024–17035.

[26] Ohkubo, K.; Kobayashi, T.; Fukuzumi, S. Direct Oxygenation of Benzene to Phenol Using Quinolinium Ions asHomogeneous Photocatalysts. *Angew. Chem., Int. Ed.* **2011**, *50*, 8652–8655.

[27] Li, P.; Deetz, A. M.; Hu, J.; Meyer, G. J.; Hu, K. Chloride Oxidation by One- or Two-Photon Excitation of *N*-Phenylphenothiazine. *J. Am. Chem. Soc.* **2022**, *144*, 17604–17610.

[28] Lepori, M.; Simon Schmid, S.; Barham, J. P. Photoredox catalysis harvesting multiple photon or electrochemical energies. *Beilstein J. Org. Chem.* **2023**, *19*, 1055–1145.

[29] Zähringer, T. J. B.; Wienhold, M.; Gilmour, R.; Kerzig, C. Direct Observation of Triplet States in the Isomerization of Alkenylboronates by Energy Transfer Catalysis. *J. Am. Chem. Soc.* **2023**, *145*, 21576–21586.

[30] Kavarnos, G. J.; Turro, N. J. Photosensitization by reversible electron transfer: theories, experimental evidence, and examples. *Chem. Rev.* **1986**, *86*, 401–449.

[31] (a) Ripak, A.; Kreijger, S. D.; Sampaio, R. N.; Vincent, C. A.; Cauët, É.; Jabin, I.; Tambar, U. K.; Elias, B.; Troian-Gautier, L. Photosensitized activation of diazonium derivatives for C–B bond formation. *Chem Catal.* **2023**, *3*, 100490. (b) Bürgin, T. H.; Glaser, F.; OliverS. Wenger, O. S. Shedding Lighton the Oxidizing Properties of Spin-Flip Excited States in a CrIII Polypyridine Complex and Their Use in Photoredox Catalysis. *J. Am. Chem. Soc.* **2022**, *144*, 14181–14194. (c) Neumann, S.; Wenger, O. S.; Kerzig, C. Controlling Spin-Correlated Radical Pairs with Donor–Acceptor Dyads: A New Concept to Generate Reduced Metal Complexes for More Efficient Photocatalysis. *Chem. Eur. J.* **2021**, *27*, 4115–4123. (d) Aydogan, A.; Bangle, R. E.; Cadranel, A.; Turlington, M. D.; Conroy, D. T.; Cauët, E.; Singleton, M. L.; Meyer, G. J.; Sampaio, R. N.; Elias, B.; Troian-Gautier, L. Accessing Photoredox Transformations with an Iron(III) Photosensitizer and Green Light. *J. Am. Chem. Soc.* **2021**, *143*, 15661–15673. (e) Gardner, J. M.; Abrahamsson, M.; Farnum, B. H.; Gerald J. Meyer, G. J. Visible Light Generation of Iodine Atoms and I-I Bonds:Sensitized I$^-$ Oxidation and I^{3-} Photodissociation. *J. Am. Chem. Soc.* **2009**, *131*, 16206–16214.

[32] Heath, G. A.; Yellowlees, L. J.; Braterman, P. S. Spectro-electrochemical studies on tris-bipyridyl ruthenium complexes; ultra-violet, visible, and near-infrared spectra of the series [Ru(bipyridyl)$_3$]$^{2+/1+/0/1-}$. *J. Chem. Soc. Chem. Comm* **1981**, 287–289.

[33] (a) Tran, T-T.; Ha-Thi, M-H.; Pino, T.; Quaranta, A.; Lefumeux, C.; Leibl, W.; Aukauloo, A. Snapshots of Light Induced Accumulation of Two Charges on Methylviologen using a Sequential Nanosecond Pump−Pump Photoexcitation. *J. Phys. Chem. Lett.* **2018**, *9*, 1086–1091. (b) Khnayzer, R. S.; Thoi, V. S.; Nippe, M.; King, A. E.; Jurss, J. W.; El Roz, K. A.; Long, J. R.; Chang, C. J.; Castellano, F. N. Towards a comprehensive understanding of visible-light photogeneration of hydrogen from water using cobalt(II) polypyridyl catalysts. *Energy Environ. Sci.* **2014**, *7*, 1477–1488.

[34] Ohkubo, K.; Mizushima, K.; Iwataa, R.; Fukuzumi, S. Selective photocatalytic aerobic bromination with hydrogen bromide via an electron-transfer state of 9-mesityl-10-methylacridinium ion. *Chem. Sci.* **2011**, *2*, 715–722.

[35] Pan, X-M.; Schuchmann, M. N.; Sonntag, C.v. Oxidation of Benzene by the OH Radical. A Product and Pulse Radiolysis Study in Oxygenated Aqueous Solution. *J. Chem. Soc. Perkin Trans. 2* **1993**, 289–297.